Effects of Unsymmetrical Stability Derivative Characteristics on Re-Entry Vehicle Trim Angle Behavior

ALBERT E. HODAPP JR.*
Sandia Laboratories, Albuquerque, N.Mex.

A quasi-steady analytical theory is developed to investigate the effects that unsymmetrical stability derivative characteristics can have on the trim angle behavior of slender rolling re-entry vehicles. For mass, aerodynamic, and inertia asymmetries, the predicted trim angle behavior patterns are more unstable near resonance than are the well-known patterns displayed by vehicles with symmetrical stability derivative characteristics. Near the resonances, small asymmetries in the static moment slope characteristics are shown to cause large, sometimes unbounded increases in trim magnification and jump discontinuities in windward meridian position. The analytically predicted trends are verified by six-degree-of-freedom numerical simulations.

Nomenclature

c.g. = center of gravity
C_A = axial force coefficient, $-F_X/q'S$
C_m = pitching moment coefficient, $M_Y/q'Sd$
C_{m_o} = aerodynamic asymmetry induced pitching moment coefficient
C_{m_q} = damping derivative coefficient, $\partial C_m/\partial(qd/2U)$, 1/rad
C_{m_α} = pitching moment slope coefficient, $\partial C_m/\partial\alpha$, 1/rad
$C_{m_{\dot\alpha}}$ = damping derivative coefficient, $\partial C_m/\partial(\dot\alpha d/2U)$, 1/rad
C_n = yawing moment coefficient, $M_Z/q'Sd$
C_{n_o} = aerodynamic asymmetry induced yawing moment coefficient
C_{n_r} = damping derivative coefficient, $\partial C_n/\partial(rd/2U)$, 1/rad
C_{n_β} = yawing moment slope coefficient, $\partial C_n/\partial\beta$, 1/rad
$C_{n_{\dot\beta}}$ = damping derivative coefficient, $\partial C_n/\partial(\dot\beta d/2U)$, 1/rad
C_Y = force coefficient for Y-body direction, $F_Y/q'S$
C_{Y_β} = force slope coefficient, $\partial C_Y/\partial\beta$, 1/rad
C_Z = force coefficient for Z-body direction, $F_Z/q'S$
C_{Z_α} = force slope coefficient, $\partial C_Z/\partial\alpha$, 1/rad
d = vehicle base diameter (Fig. 1), ft or m
F_X, F_Y, F_Z = aerodynamic forces acting along the X, Y, Z axes, respectively, lb or N
g = gravitational acceleration, ft/sec^2 or m/sec^2
G = critical frequency ratio [Eq. (16)]
h = altitude, ft or m
i = $(-1)^{1/2}$
I_X, I_Y, I_Z = moments of inertia about the X, Y, Z axes, respectively, slug-ft^2 or Kg-m^2
J_{XY}, J_{YZ}, J_{XZ} = products of inertia relative to the X, Y, Z axes, slug-ft^2 or Kg-m^2
m = vehicle mass, slugs or Kg
M_X, M_Y, M_Z = aerodynamic moments about the X, Y, Z axes, respectively, ft-lb or N-m
p, q, r = angular velocities about the X, Y, Z axes, respectively (roll, pitch, and yaw rates), rad/sec
p_{cr_p}, p_{cr_y} = pitch and yaw critical frequencies, respectively, [Eqs. (8) and (11)], rad/sec
q' = dynamic pressure, lb/ft^2 or N/m^2
S = reference area, $S = \pi d^2/4$, ft^2 or m^2
t = time, sec
U = total velocity, ft/sec or m/sec
X, Y, Z = body reference axes, mutually parallel to X_g, Y_g, Z_g axes, with origin at the c.g. (Fig. 1)
X_g, Y_g, Z_g = geometric axes, with X_g the axis of geometric symmetry (Fig. 1)
X_p, Y_p, Z_p = principal axes (Fig. 1)
$y_{c.g.}, z_{c.g.}$ = position of the c.g. relative to origin of X_g, Y_g, Z_g axes along Y_g and Z_g axes respectively (Fig. 1), ft or m
α, β = angle of attack and sideslip angle, respectively, rad or deg
α_o, β_o = reference ($p = 0$) trim angles of attack and sideslip which result from aerodynamic asymmetries, rad or deg
γ = flight path angle, deg
$\delta_\alpha, \delta_\beta$ = inclination angles between the X_p, Y_p, Z_p and X, Y, Z axes [Fig. 1 and Eqs. (1) and (2)], rad or deg
ζ = complex total angle of attack, rad or deg
λ_p, λ_y = pitch and yaw roll rate ratios, respectively [Eqs. (7) and (10)]
μ_p, μ_y = pitch and yaw damping ratios, respectively [Eqs. (9) and (12)]
ρ = atmospheric density, slug/ft^3 or Kg/m^3
ϕ = aerodynamic roll angle, trim orientation angle, or windward meridian position [Eq. (15) and Fig. 2], rad or deg
$\|\ \|$ = absolute value or magnitude
$\dot{(\ )}, \ddot{(\ )}$ = first and second derivatives with respect to time

Subscripts
i, R, T = initial, reference, and trim conditions

Introduction

MANY investigations concerning the trim angle behavior of slender rolling re-entry vehicles can be found in Refs. 1–7. In these investigations, the effects of various types of small trim producing asymmetries were studied using the assumption that the stability derivative coefficients of the re-entry vehicle are symmetrical; i.e., $C_{Z_\alpha} = C_{Y_\beta}$, $C_{m_\alpha} = -C_{n_\beta}$, $C_{m_q}+C_{m_{\dot\alpha}} = C_{n_r}-C_{n_{\dot\beta}}$, etc. Walchner[8] has shown experimentally that at hypersonic speeds small nosetip asymmetries on otherwise symmetrical conical vehicles can introduce flowfield pressure perturbations which, in addition to creating trim angles, invalidate the symmetrical aerodynamic stability derivative assumption. To the author's knowledge, investigations of this effect of small asymmetries on re-entry vehicle trim angle behavior have not appeared in the literature. A detailed description is given herein of the effects unsymmetrical stability derivative characteristics ($C_{Z_\alpha} \neq C_{Y_\beta}$, $C_{m_\alpha} \neq -C_{n_\beta}$, $C_{m_q}+C_{m_{\dot\alpha}} \neq C_{n_r}-C_{n_{\dot\beta}}$, etc.) have on the trim angle behavior of slender rolling re-entry vehicles. For these vehicles, it is shown that trim angle behavior near resonance

Received November 6, 1973; revision received January 9, 1974. This work was supported by the U.S. Atomic Energy Commission. The author wishes to thank G. E. Reis, J. R. Kelsey, and G. W. Stone of Sandia Laboratories for their assistance and suggestions.

Index categories: Entry Vehicle Dynamics and Control; LV/M Dynamics and Control.

* Member of the Technical Staff, Aerodynamics Projects Department. Member AIAA.

can become more unstable than the trim angle behavior displayed by vehicles which have symmetrical stability derivative characteristics and equivalent trim producing asymmetries. Because of increased trim magnification and changes in windward meridian behavior near resonance, the presence of unsymmetrical stability derivative characteristics can invalidate trim magnitude predictions and predictions of trim induced roll rate behavior that are based on previous analytical results for re-entry vehicles.

A quasi-steady analytical theory is developed to provide an insight into the effects of unsymmetrical stability derivative characteristics on the trim angle behavior of slender rolling re-entry vehicles. Results similar to those developed herein were obtained for a rolling airplane by Rhoads and Schuler[9]; however, their analytical results do not include all of the trim-producing effects which must be considered for re-entry vehicle flights. The effects of small mass asymmetries (c.g. offset), aerodynamics asymmetries (C_{m_o} and/or C_{n_o}), and inertia asymmetries (principal axis misalignment) are included in the analytical results presented here. Six-degree-of-freedom (6-DOF) simulations are presented to confirm the analytically predicted trends. Walchner's experimental results are used as a guide to obtain realistic bounds on the asymmetries of the stability derivative coefficients used for the examples, simulations, and comparisons included in this presentation.

Theoretical Analysis

Equations of Angular Motion

The following differential equations describe the pitching-yawing motions of a rolling re-entry vehicle that has unsymmetrical stability derivative characteristics and small mass, aerodynamic, and inertia asymmetries.

$$\ddot{\alpha}+A_\alpha\dot{\alpha}+B_\alpha\alpha+C_\alpha\ddot{\beta}+D_\alpha\dot{\beta}+E_\alpha\beta=F_\alpha \tag{1}$$

where

$$A_\alpha=-\left(\frac{q'S}{mU}\right)\left[(C_A+C_{Z_\alpha})+\frac{md^2}{2I_Y}(C_{m_q}+C_{m_{\dot\alpha}})\right]$$

$$B_\alpha=-\frac{q'Sd}{I_Y}C_{m_\alpha}-\left(\frac{I_Z-I_X}{I_Y}\right)p^2$$

$$C_\alpha=\frac{J_{YZ}}{I_Y}$$

$$D_\alpha=p\left[1+\left(\frac{I_Z-I_X}{I_Y}\right)\right]$$

$$E_\alpha=-p\left(\frac{q'S}{mU}\right)\left[\left(\frac{I_Z-I_X}{I_Y}\right)(C_A+C_{Y_\beta})+\frac{md^2}{2I_Y}C_{m_q}\right]+\frac{J_{YZ}}{I_Y}p^2$$

$$F_\alpha=\frac{q'Sd}{I_Y}\left[C_{m_o}+C_A\left(\frac{z_{\text{c.g.}}}{d}\right)\right]-\left(\frac{I_Z-I_X}{I_Y}\right)\delta_\alpha p^2 \quad \text{and}$$

$$\delta_\alpha=J_{XZ}/(I_Z-I_X)$$

$$\ddot{\beta}+A_\beta\dot{\beta}+B_\beta\beta+C_\beta\ddot{\alpha}+D_\beta\dot{\alpha}+E_\beta\alpha=F_\beta \tag{2}$$

where

$$A_\beta=-\left(\frac{q'S}{mU}\right)\left[(C_A+C_{Y_\beta})+\frac{md^2}{2I_Z}(C_{n_r}-C_{n_{\dot\beta}})\right]$$

$$B_\beta=\frac{q'Sd}{I_Z}C_{n_\beta}-\left(\frac{I_Y-I_X}{I_Z}\right)p^2$$

$$C_\beta=J_{YZ}/I_Z$$

$$D_\beta=-p\left[1+\left(\frac{I_Y-I_X}{I_Z}\right)\right]$$

$$E_\beta=p\left(\frac{q'S}{mU}\right)\left[\left(\frac{I_Y-I_X}{I_Z}\right)(C_A+C_{Z_\alpha})+\frac{md^2}{2I_Z}C_{n_r}\right]+\frac{J_{YZ}}{I_Z}p^2$$

$$F_\beta=-\frac{q'Sd}{I_Z}\left[C_{n_o}-C_A\left(\frac{y_{\text{c.g.}}}{d}\right)\right]-\left(\frac{I_Y-I_X}{I_Z}\right)\delta_\beta p^2 \quad \text{and}$$

$$\delta_\beta=J_{XY}/(I_Y-I_X)$$

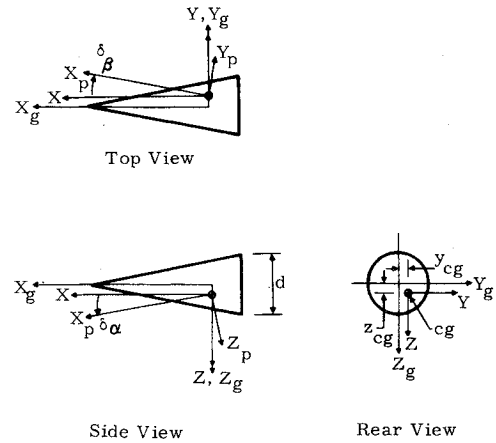

Fig. 1 Coordinate systems and nomenclature.

These coupled differential equations were derived using the X, Y, Z body fixed axis system (Fig. 1) as a reference. The assumptions used in developing the equations are as follows:

a) Gravitational acceleration and asymmetry induced forces have a negligible effect on the angular motions of the re-entry vehicle.

b) The re-entry vehicle experiences only small perturbations in angle of attack and side-slip angle (α and $\beta \ll 1$ rad).

c) Aerodynamic forces and moments vary linearly with α, β, q, r, and the time derivatives of α and β.

d) The products of inertia J_{XY}, J_{XZ}, and J_{YZ} are small compared to the moments of inertia I_X, I_Y, and I_Z; and

e) Mass and aerodynamic asymmetries are small ($|y_{\text{c.g.}}/d|$ and $|z_{\text{c.g.}}/d| \ll 1$; $|C_{m_o}/C_{m_\alpha}|$ and $|C_{n_o}/C_{n_\beta}| \ll 1$).

The forcing functions F_α and F_β in Eqs. (1) and (2) contain the parameters which cause the re-entry vehicle to trim at a non-zero angle relative to the wind. Contributors to the total trim angle of attack are mass asymmetries $y_{\text{c.g.}}$ and $z_{\text{c.g.}}$, aerodynamic asymmetry induced pitching and yawing moment coefficients C_{m_o} and C_{n_o}, and inertia asymmetries δ_α and δ_β.

The coefficients F_α and F_β are separated into two distinct groups of parameters. The group that results from inertia asymmetry is multiplied by the roll rate squared; the remaining group in each of these coefficients contains the mass and aerodynamic asymmetry terms. This grouping of parameters indicates that the trim angles that result from mass and aerodynamic asymmetries will display similar behavior, whereas the inertia asymmetry induced trim angle will display a distinctly different behavior.[7]

During flight the coefficients of Eqs. (1) and (2) are variables because of altitude and velocity changes. For the quasi-steady theoretical results presented here, it is assumed that the variation of these coefficients with respect to time is such that they can be considered essentially constant over small time intervals of the flight. The solutions for the transient angular motions are ignored because only the trim angle behavior is being considered in this development. The solutions of Eqs. (1) and (2) then reduce to the steady response or particular solutions of these linear second-order equations which are given as

$$\alpha_T=(F_\alpha B_\beta-E_\alpha F_\beta)/(B_\alpha B_\beta-E_\alpha E_\beta) \tag{3}$$

and

$$\beta_T=(F_\beta B_\alpha-E_\beta F_\alpha)/(B_\alpha B_\beta-E_\alpha E_\beta) \tag{4}$$

The terms on the right-hand side of Eqs. (3) and (4) are defined in Eqs. (1) and (2).

A consequence of assuming that the coefficients of Eqs. (1) and (2) are constant is that Eqs. (3) and (4) will always predict the steady-state trim angles at each value of time. This is equivalent to having a trim angle that responds instantaneously to the forcing function. During flight, the trim angle requires a

finite time to build up and therefore cannot respond instantaneously. For this reason, differences in the magnitudes of the theoretically predicted trim angle and the actual trim angle exist. These differences are largest during high altitude transient resonance encounters. For conditions of sustained resonance and for transient resonance conditions at low altitudes, these differences can be quite small.

Trim Angle of Attack

After some algebraic manipulation of Eqs. (3) and (4), the expressions for the trim angle of attack and the trim angle of sideslip can be reduced to

$$\alpha_T = \frac{(\alpha_{T_R}-\delta_\alpha\lambda_p^2)(1-\lambda_y^2)-(\beta_{T_R}-\delta_\beta\lambda_y^2)\left[\lambda_p\mu_p+\lambda_p^2\left(\frac{J_{YZ}}{I_Z-I_X}\right)\right]}{(1-\lambda_y^2)(1-\lambda_p^2)+\left[\lambda_p\mu_p+\lambda_p^2\left(\frac{J_{YZ}}{I_Z-I_X}\right)\right]\left[\lambda_y\mu_y-\lambda_y^2\left(\frac{J_{YZ}}{I_Y-I_X}\right)\right]} \tag{5}$$

$$\beta_T = \frac{(\beta_{T_R}-\delta_\beta\lambda_y^2)(1-\lambda_p^2)+(\alpha_{T_R}-\delta_\alpha\lambda_p^2)\left[\lambda_y\mu_y-\lambda_y^2\left(\frac{J_{YZ}}{I_Y-I_X}\right)\right]}{(1-\lambda_y^2)(1-\lambda_p^2)+\left[\lambda_p\mu_p+\lambda_p^2\left(\frac{J_{YZ}}{I_Z-I_X}\right)\right]\left[\lambda_y\mu_y-\lambda_y^2\left(\frac{J_{YZ}}{I_Y-I_X}\right)\right]} \tag{6}$$

where α_{T_R} and β_{T_R} are the reference trim angles which result from mass and aerodynamic asymmetry; δ_α and δ_β are the reference trim angles which result from inertia asymmetry; and

$$\lambda_p = p/p_{crp} \tag{7}$$

$$p_{crp} = \pm[-C_{m_\alpha}q'Sd/(I_Z-I_X)]^{1/2} \tag{8}$$

$$\mu_p = \pm\left\{-\rho^{1/2}S\left[\frac{1}{2m}(C_A+C_{Y_\beta})+\frac{d^2}{4}\left(\frac{C_{m_q}+C_{m_{\dot\alpha}}}{I_Z-I_X}\right)\right]\Big/\left[\frac{-C_{m_\alpha}Sd}{2(I_Z-I_X)}\right]^{1/2}\right\} \tag{9}$$

$$\lambda_y = p/p_{cry} \tag{10}$$

$$p_{cry} = \pm[C_{n_\beta}q'Sd/(I_Y-I_X)]^{1/2} \tag{11}$$

and

$$\mu_y = \pm\left\{-\rho^{1/2}S\left[\frac{1}{2m}(C_A+C_{Z_\alpha})+\frac{d^2}{4}\left(\frac{C_{n_r}-C_{n_{\dot\beta}}}{I_Y-I_X}\right)\right]\Big/\left[\frac{C_{n_\beta}Sd}{2(I_Y-I_X)}\right]^{1/2}\right\} \tag{12}$$

The signs of p_{crp} and p_{cry} are always the same as that of p; therefore, the roll rate ratios λ_p and λ_y are always positive. Similarly, the signs outside the brackets in the expressions for the damping ratios μ_p and μ_y are the same as that of p. The aerodynamic coefficients combine to yield a positive term within the brackets of Eqs. (9) and (12) for re-entry configurations of interest; then, μ_p and μ_y have the sign of the roll rate.

The total trim angle of attack ζ_T (Fig. 2) may be defined in terms of α_T and β_T [Eqs. (5) and (6)] as follows:

$$\zeta_T = |\zeta_T|(\sin\phi + i\cos\phi) = \beta_T + i\alpha_T \tag{13}$$

where the total trim angle magnitude

$$|\zeta_T| = (\beta_T^2+\alpha_T^2)^{1/2} \tag{14}$$

and the orientation angle or windward meridian position

$$\phi = \tan^{-1}(\beta_T/\alpha_T) \tag{15}$$

The reference roll rate condition for mass and/or aerodynamic asymmetry induced trim angle is $p = 0$. At $p = 0$, $\zeta_T = (\beta_{T_R}+i\alpha_{T_R})$, where

$$\alpha_{T_R} = \alpha_o-(C_A/C_{m_\alpha})(z_{c.g.}/d)$$

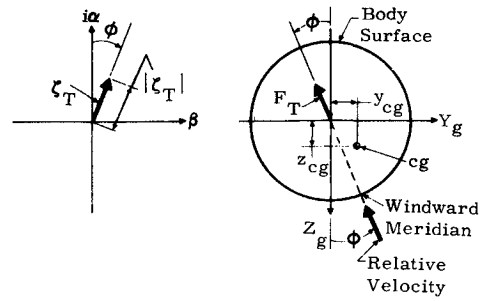

Fig. 2 Orientation of total trim angle, lateral trim force, and windward meridian.

and

$$\beta_{T_R} = \beta_o+(C_A/C_{n_\beta})(y_{c.g.}/d)$$

The quantities α_o and β_o are the nonrolling angle of attack and side-slip angle caused by aerodynamic asymmetries: $\alpha_o = -C_{m_o}/C_{m_\alpha}$; $\beta_o = -C_{n_o}/C_{n_\beta}$.

The reference roll rate condition for the inertia asymmetry induced trim angle is $p \to \infty$. Neglecting the products of principal axis inclination angles, $\zeta_T \to (\delta_\beta + i\delta_\alpha)$ as $p \to \infty$. The reference trim angles δ_α and δ_β are defined in terms of the moments and products of inertia in Eqs. (1) and (2).

Trim Angle Behavior

Equations (5) and (6) contain the effects of unsymmetrical stability derivative characteristics as well as previously unreported effects of the J_{YZ} product of inertia. This product of inertia introduces an additional damping or undamping effect into the denominators of these equations. These identical denominators can go to zero at or near the undamped resonances $\lambda_p = 1$ and $\lambda_y = 1$; therefore, near these undamped resonances α_T, β_T and hence $|\zeta_T|$ [Eq. (14)] can become unbounded. If the roll rate ratios λ_p and λ_y are unequal and/or if J_{YZ} is nonzero, zeros can occur in the denominators of Eqs. (5) and (6) even when the damping ratios μ_p and μ_y are nonzero. Previous descriptions of re-entry vehicle trim angle behavior[1-7] require only that the damping ratio be nonzero for trim magnification to remain finite. The presence of an unbounded or even large trim angle violates the small angle restriction on the applicability of these expressions. Even so, this analytical prediction cannot be ignored because it indicates the possible occurrence of a serious instability. It is shown later that very unstable trim angle behavior can occur in flight as indicated by the analytical expressions.

Note that for nonzero J_{YZ} even so-called symmetrical vehicles (i.e., vehicles having $\lambda_p = \lambda_y$, $\mu_p = \mu_y$, $I_Y = I_Z$) can experience unbounded trim angle near resonance when aerodynamic damping is present. There are conditions for which J_{YZ} can have a significant effect on trim angle behavior; however, for realistic values of this parameter, these effects are small when compared to those which result from small asymmetries in some stability derivative coefficients. The effects on trim angle behavior of the J_{YZ} product of inertia are a separate subject and are not discussed further here. The present discussion is confined to describing some of the more important effects that unsymmetrical stability derivative coefficient characteristics can have on trim angle behavior.

In order to simplify the description of trim angle behavior in the presence of unsymmetrical stability derivative coefficients, it will be assumed that $J_{YZ} = 0$ and that there is a constant difference in the magnitudes of C_{m_α} and C_{n_β}. This second assumption yields the following linear relationship between the two roll rate ratios

$$\lambda_y = G\lambda_p \tag{16}$$

where the critical frequency ratio G (a constant) is given as

$$G = [-C_{m_\alpha}(I_Y - I_X)/C_{n_\beta}(I_Z - I_X)]^{1/2}$$

Using Eq. (16) and letting $J_{YZ} = 0$, Eqs. (5) and (6) reduce to

$$\alpha_T = \frac{(\alpha_{T_R} - \delta_\alpha \lambda_p^2)(1 - G^2\lambda_p^2) - (\beta_{T_R} - \delta_\beta G^2 \lambda_p^2)\lambda_p \mu_p}{(1 - G^2\lambda_p^2)(1 - \lambda_p^2) + G\lambda_p^2 \mu_p \mu_y} \quad (17)$$

and

$$\beta_T = \frac{(\beta_{T_R} - \delta_\beta G^2\lambda_p^2)(1 - \lambda_p^2) + (\alpha_{T_R} - \delta_\alpha \lambda_p^2)G\lambda_p \mu_y}{(1 - G^2\lambda_p^2)(1 - \lambda_p^2) + G\lambda_p^2 \mu_p \mu_y} \quad (18)$$

The total trim angle of attack ζ_T is obtained after substituting Eqs. (17) and (18) into Eq. (13). The behavior of the magnitude $|\zeta_T|$ and the orientation ϕ of the total trim angle is investigated by varying λ_p while holding μ_p, μ_y, and G constant. The denominator of $|\zeta_T|$, which is identical to those of Eqs. (17) and (18), is quadratic in λ_p^2. To find the values of λ_p which cause $|\zeta_T|$ to become undefined, the denominator is set equal to zero and the resulting biquadratic equation is solved for its roots. When positive real roots exist, they must satisfy

$$\lambda_p = \frac{1}{G}\left(\frac{G^2 - G\mu_p\mu_y + 1}{2}\right)^{1/2}\left\{1 \pm \left[1 - \left(\frac{2G}{G^2 - G\mu_p\mu_y + 1}\right)^2\right]^{1/2}\right\}^{1/2} \quad (19)$$

Since G and the product $\mu_p\mu_y$ are both positive, with $\mu_p\mu_y \ll 1$, this equation indicates that when

$$2G/(G^2 - G\mu_p\mu_y + 1) \leqq 1 \quad (20)$$

the roots are real, and therefore zeroes can occur in the denominator of $|\zeta_T|$ at positive real values of λ_p. For re-entry vehicles, these zeroes occur very close to the undamped resonance conditions $\lambda_p = 1$ and $\lambda_y = G\lambda_p = 1$; therefore, $|\zeta_T|$ can become unbounded near these conditions. Note that when $G \neq 1$ and/or when μ_p and $\mu_y \neq 0$, zeroes cannot occur simultaneously in the numerator and denominator of $|\zeta_T|$.

The product of damping ratios $\mu_p\mu_y$ has a strong influence on the range of G over which the trim magnitude remains bounded near resonance. This is shown in Fig. 3 where the left-hand side of Eq. (20) is plotted vs G for selected values of $\mu_p\mu_y$. According to Eq. (20), the horizontal line on Fig. 3 separates the regions of bounded (imaginary λ_p above the line) and unbounded (positive real λ_p at and below the line) trim angle. Each member of the family of curves ($\mu_p\mu_y = \text{const}$) presented in Fig. 3 intersects this horizontal line. The distance along the line between intersections defines the range of G over which the trim angle will remain bounded as λ_p varies. Notice that as the magnitude of the product $\mu_p\mu_y$ increases, this range of G increases. Equations (9) and (12) show that μ_p and μ_y are directly proportional to $\rho^{1/2}$; therefore, as altitude decreases μ_p and μ_y increase in magnitude. Consequently, the range of G for bounded trim angle near resonance increases with decreasing altitude.

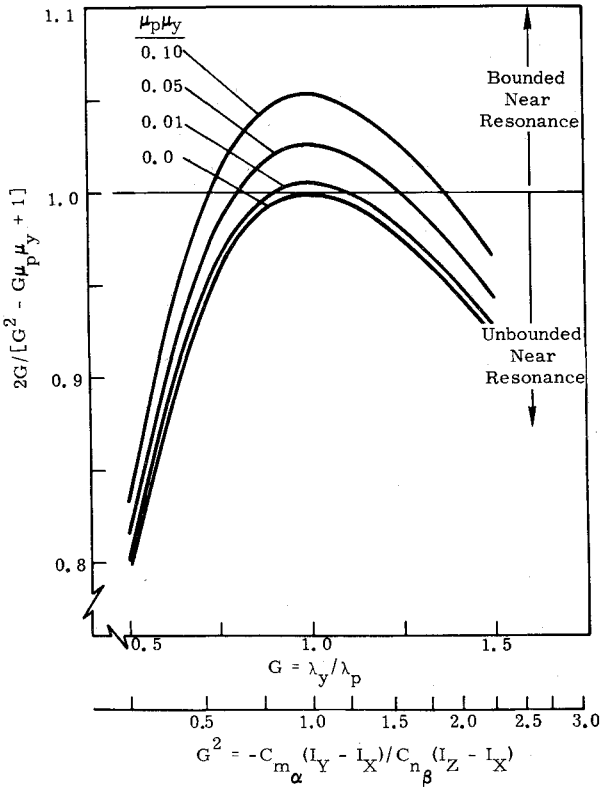

Fig. 3 Parameters which influence trim angle magnitude.

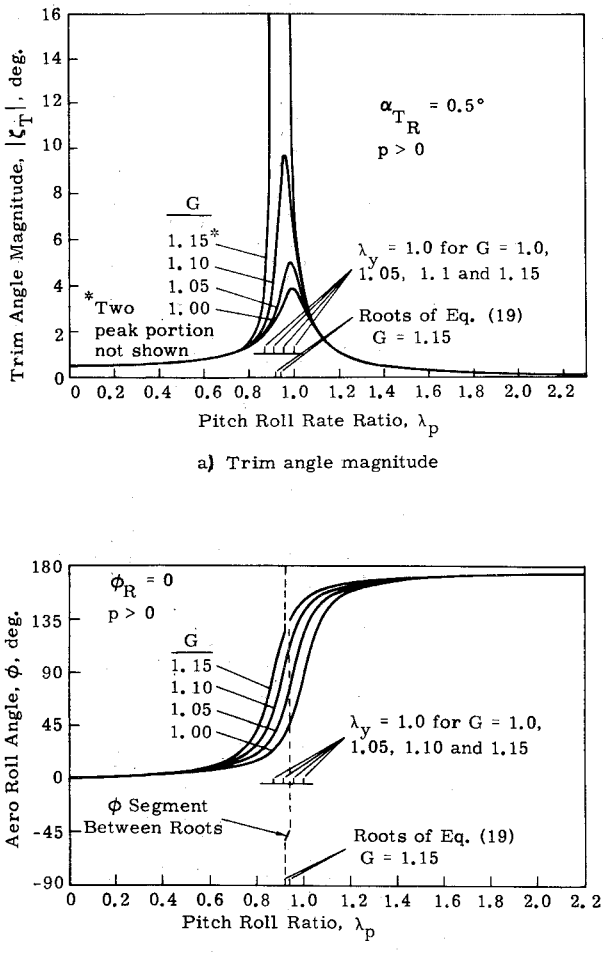

Fig. 4 Low altitude trim angle response to mass and/or aerodynamic asymmetry and static moment slope asymmetry.

Asymmetries in the static force slope coefficients and damping derivative coefficients can contribute to unstable trim angle behavior through their effect on the damping ratios μ_p and μ_y; however, the dominant effect of unsymmetrical stability derivative coefficient characteristics on trim angle behavior is that which results from differences in the pitching moment slope coefficient and yawing moment slope coefficient (i.e., when $C_{m_\alpha} \neq -C_{n_\beta}$). This effect on trim angle behavior is illustrated in Figs. 4 and 5 for a mass and/or aerodynamic asymmetry induced trim angle. The components of this trim angle $|\zeta_T|$ and ϕ, are presented as functions of λ_p and G. The trim angle behavior presented in Figs. 4 and 5 is representative of that which could occur at altitudes near those where a ballistic re-entry vehicle encounters low altitude and high altitude resonance, respectively.

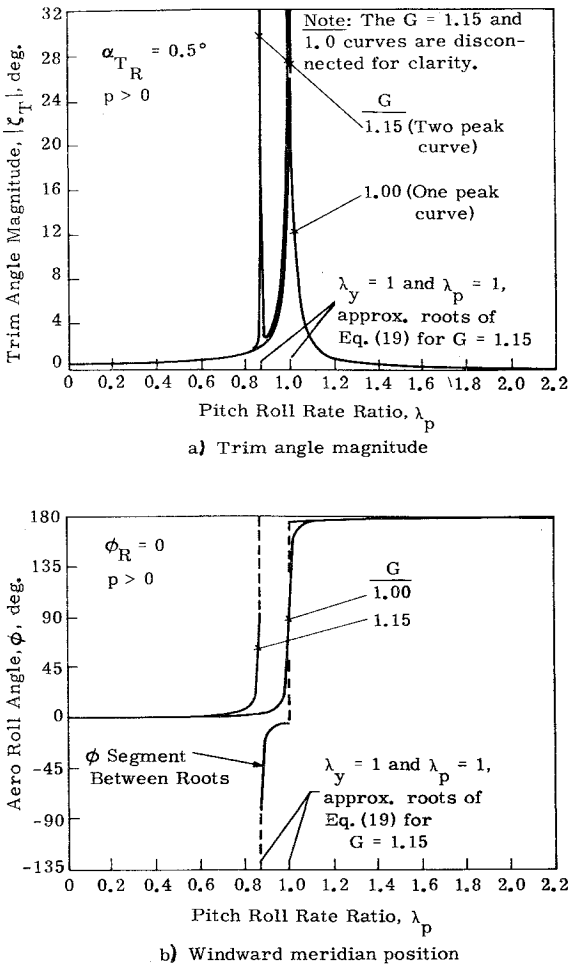

Fig. 5 High altitude trim angle response to mass and/or aerodynamic asymmetry and static moment slope asymmetry.

The vehicle used to generate these curves is a 10° cone that has a reference trim angle of attack α_{T_R} of 0.5°. The vehicle is symmetrical except for the small trim producing asymmetries and for differences in C_{m_α} and C_{n_β}; i.e., $I_Y = I_Z$, $C_{Y_\beta} = C_{Z_\alpha}$, $C_{m_q} + C_{m_{\dot\alpha}} = C_{n_r} - C_{n_{\dot\beta}}$, and $C_{m_\alpha} = -G^2 C_{n_\beta}$. The pitching moment slope coefficient was held constant while C_{n_β} was varied using G values of 1.0, 1.05, 1.1, and 1.15. This corresponds to differences in C_{m_α} and C_{n_β} of 0%, 10%, 21%, and 32%, all of which fall within the range reported by Walchner.[8] Because C_{m_α} is constant, α_{T_R} remains constant as G is varied. The $G = 1$ curves in Figs. 4 and 5 are the reference curves since they describe the trim angle behavior of a re-entry vehicle that has symmetrical force and moment stability derivative coefficients. As shown in Figs. 4 and 5 the variation in G has little effect on trim angle behavior relative to the $G = 1$ curves for values of λ_p away from the undamped resonances $\lambda_p = 1$ and $\lambda_p = G^{-1}$; however, near these resonances there is a very large effect. In Figs. 4 and 5, the variation in G is presented only for values ≥ 1. This is because a similar range of G over values ≤ 1 will yield similar trim angle behavior.

As G increases from one, the aerodynamic static moment slope characteristics of the re-entry vehicle become more unsymmetrical and, as shown in Fig. 4a, the magnification of the total trim angle is increased significantly near the undamped resonances. The maximum amplitude occurs between these resonances because of the influence of the aerodynamic damping. As the trim magnification increases, $|\zeta_T|$ evolves from a single peak curve into a double peak curve (not shown in Fig. 4a); one peak then becomes unbounded followed immediately by the second. For the low altitude condition depicted in Fig. 4a, Eq. (20) can be used to show that the $|\zeta_T|$ vs λ_p curves will remain bounded for $0.905 < G < 1.105$ (Fig. 3, $\mu_p \mu_y = 0.01$); i.e., the curves will remain bounded for differences in the magnitudes of C_{m_α} and C_{n_β} of less than 22% (Fig. 3, recall that $I_Y = I_Z$). In Fig. 4a, it is shown that $|\zeta_T|$ is bounded for $G = 1.05$ and 1.10, but becomes unbounded when G is increased to 1.15 ($-C_{m_\alpha}/C_{n_\beta} = 1.32$). The values of λ_p at which $|\zeta_T|$ becomes undefined [positive real roots of Eq. (19)] are indicated for the $G = 1.15$ curves in both Figs. 4 and 5.

At the high altitude condition where the aerodynamic damping is considerably smaller (Fig. 5, $\mu_p \mu_y = 0.0002$), Eq. (20) indicates that the $|\zeta_T|$ vs λ_p curves will remain bounded only for $0.986 < G < 1.014$; i.e., only for differences in the magnitudes of C_{m_α} and C_{n_β} of less than 2.8%. The two peak $|\zeta_T|$ vs λ_p curve for $G = 1.15$ in Fig. 5a therefore is representative of trim angle behavior at high altitudes for almost all values of $G > 1$; however, values of G smaller than 1.15 will cause the two divergent peaks to move closer together. Because the aerodynamic damping is very small at high altitudes, $|\zeta_T|$ becomes unbounded at values of λ_p which are very close to those for the undamped resonances.

The effects of unsymmetrical static moment slope characteristics on windward meridian (ϕ) behavior are shown in Figs. 4b and 5b. When $G > 1$ but small enough for $|\zeta_T|$ to remain bounded ($G = 1.05$ and 1.10 in Fig. 4b), the ϕ vs λ_p curves are simply shifted relative to the $G = 1$ curve with the 180° range of ϕ remaining unchanged. At values of λ_p where $|\zeta_T|$ becomes undefined [positive real roots of Eq. (19)], jump discontinuities result in the ϕ vs λ_p curves (Figs. 4b and 5b, $G = 1.15$) which

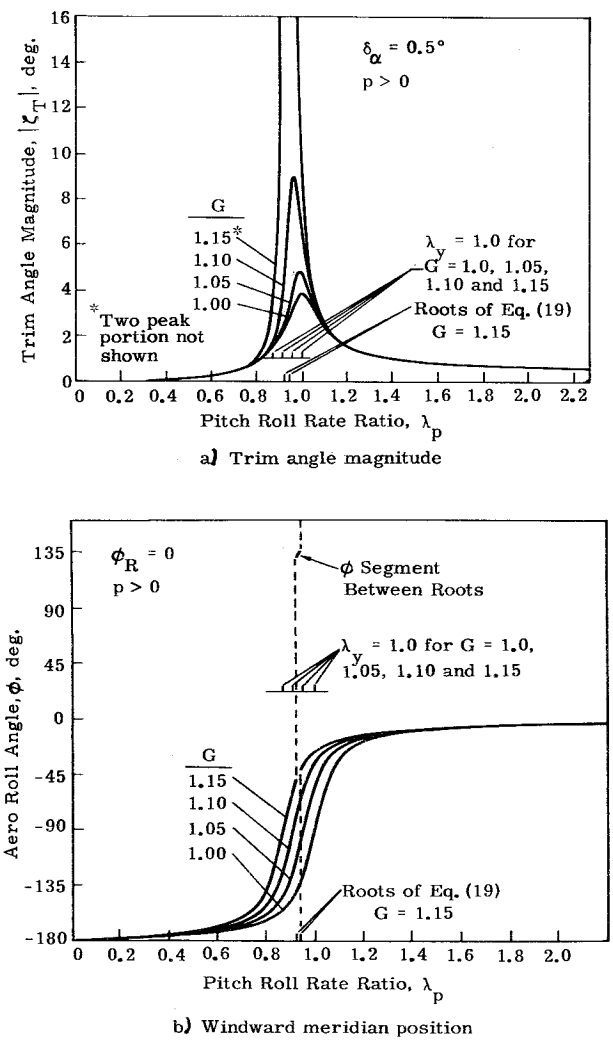

Fig. 6 Low altitude trim angle response to inertia asymmetry and static moment slope asymmetry.

cause a 180° shift in the windward meridian position; i.e., the body rolls over relative to the wind. Between these discontinuities, the windward meridian position ϕ varies with λ_p in a normal manner except for the 180° bias.

The results given in Figs. 4b and 5b ($\mu_p, \mu_y > 0$) indicate that positive changes in λ_p produce positive changes in ϕ even over the range of λ_p values between discontinuities. Excluding this small range of λ_p values between discontinuities, the windward meridian behavior for re-entry vehicles having $G \leqq 1$ or $G \geqq 1$ is similar ($G \geqq 1$ is shown); i.e., there is a 180° change in ϕ as the roll rate ratio is varied from $\lambda_p \ll 1$ to $\lambda_p \gg 1$; also, a 90° change in ϕ occurs in going from a reference roll rate condition ($\lambda_p = 0$ or $\lambda_p \to \infty$) to one of the undamped resonance conditions. For the cases presented in Figs. 4b and 5b, a reference trim angle of attack (α_{T_R}) was used; therefore, the 90° change in windward meridian position occurs as λ_p is varied from zero to G^{-1}, the value at the undamped yaw resonance. If a reference trim angle of sideslip (β_{T_R}) had been used, the 90° change in ϕ would have occurred at the undamped pitch resonance ($\lambda_p = 1$).

An example is presented in Fig. 6 to demonstrate the trim angle behavior of a re-entry vehicle that has an inertia asymmetry and unsymmetrical static moment slope characteristics. The reference vehicle used to generate the curves in Fig. 6 is identical to the vehicle used to generate the curves presented in Fig. 4, with the exception of the type of trim producing asymmetry. The same low altitude reference condition was used in both figures, and the reference trim angles have the same numerical value ($\alpha_{T_R} = \delta_\alpha = 0.5°$). The results presented in Figs. 4 and 6 can be compared for equivalent values of G to demonstrate the different trim angle behavior patterns induced by these different types of trim producing asymmetries.

Before making these comparisons, there are some general relationships between these two basic types of trim angles that should be mentioned. In order to discuss these relationships, subscript 1 will be used to indicate the inertia asymmetry induced trim angle components and subscript 2 will be used to identify components of the trim angle which results from the presence of mass and/or aerodynamic asymmetries. When the reference values of these two types of trim angles satisfy the relationship

$$\delta_\alpha \beta_{T_R} - \alpha_{T_R} \delta_\beta G^2 = 0 \tag{21}$$

the windward meridian positions differ by a constant angular displacement

$$\phi_1 = \phi_2 + C \tag{22}$$

for all values of λ_p, and the total trim angle magnitudes at the undamped resonances are related by

$$|\zeta_{T_1}| = G^n |\zeta_{T_2}| \tag{23}$$

The values of n are given in Table 1. Equation (21) governs the choice of signs for the reference angles in Table 1 and K is a constant.

Table 1 Values of n for Eq. (23)

Reference trim angle relations Eq. (21)	$\lambda_p = 1$	$\lambda_p = G^{-1}$
$\alpha_{T_R} = \pm K\delta_\alpha$ $\beta_{T_R} = \pm K\delta_\beta G^2$	$n = 0$	$n = -2$
$\delta_\alpha = \pm K\alpha_{T_R} G^2$ $\delta_\beta = \pm K\beta_{T_R}$	$n = 2$	$n = 0$

The reference conditions used for Figs. 4 and 6 ($\delta_\alpha = \alpha_{T_R} = 0.5°$, $\beta_{T_R} = \delta_\beta = 0$) satisfy Eq. (21). For these particular reference conditions $C = 180°$ in Eq. (22) for all λ_p, while $n = 0$ and -2 in Eq. (23) at $\lambda_p = 1$ and G^{-1}, respectively. Between the undamped resonances, the differences in the maximum magnitudes of the two trim angles increases as G increases from one, with the maximum magnitude of the mass and/or aerodynamic asymmetry induced trim angle (Fig. 4a) being the larger. If G were decreased from one, the differences in maximum magnitude would again increase; however, then the maximum magnitude of the inertia asymmetry induced trim angle would be largest. For $G = 1$, the maximum magnitudes are equal. At conditions far above and far below resonance ($\lambda_p \gg 1$ and $\lambda_p \ll 1$), where variations in G have no effect (Figs. 4 and 6), the two types of trim angle have opposite asymptotic behavior[7]; i.e., as one approaches its reference value, the other approaches zero.

Digital 6-DOF Simulations

The preceding theoretical development provides an analytical tool by which a more complete knowledge can be gained concerning the effects of unsymmetrical stability derivative coefficients on the trim angle behavior of slender rolling re-entry vehicles. These quasi-steady analytical results indicate that the largest effect of unsymmetrical stability derivatives is that of unsymmetrical static moment slope coefficients ($C_{m_z} \neq -C_{n_\beta}$). The theoretical results indicate that increasing the asymmetry of the static moment slope characteristics increases the trim magnification near resonance and when differences in C_{m_z} and C_{n_β} exceed some altitude dependent limit, unbounded trim magnification occurs accompanied by jump discontinuities in the windward meridian position. In order to investigate these analytical predictions, re-entry simulations were obtained by numerically integrating the complete 6-DOF equations of motion. The results of these simulations are presented in this section.

The reference vehicle used for the re-entry simulations was the Sandia Re-entry Vehicle Resonance Test Vehicle (RVRTV), a 10° half-angle cone having a 1.25 ft (0.381 m) base diameter, a nose to base radius ratio of 0.0167, a 6% hypersonic static margin and a Newtonian ballistic coefficient of approximately 1100 lb/ft^2 (5.267×10^4 N/m^2). The external geometry of this vehicle is the same as standard dynamic stability calibration models used by the Supersonic Tunnel Association and the AGARD.[16] For these simulations the vehicle is symmetrical except for small trim producing asymmetries and for differences in C_{m_z} and C_{n_β}. The aerodynamic stability derivative coefficients of the reference vehicle were held constant to be consistent with the restrictions on the theory.

The initial re-entry conditions used for these 6-DOF digital simulations were $U_i = 21{,}600$ fps (6584 m/sec), $\gamma_i = -20.6°$ and $h_i = 180{,}000$ ft (54,864 m). The initial roll rate, $p_i = 44$ rad/sec, was chosen so that the re-entry vehicle would encounter both high altitude and low altitude resonance when the roll rate remained constant.

A description, based on results obtained from the 6-DOF simulations, is given in Fig. 7 of the effect of unsymmetrical static moment slope characteristics ($G^2 = -C_{m_z}/C_{n_\beta} > 1$) on the trim angle behavior of a rolling re-entry vehicle. High altitude and low altitude resonance encounters are presented for the RVRTV with a 0.5° reference trim angle of attack (α_{T_R}). The $G = 1$ curves in Fig. 7 are the reference curves since they represent the trim angle behavior of a vehicle with symmetrical stability derivative characteristics. The roll rate remained constant throughout these simulated flights because the roll torque, M_X, was set equal to zero. Total angle-of-attack transients were eliminated during the early portion of these simulated flights by the proper choice of initial conditions. The total trim angle of attack diverged explosively for some high altitude resonance encounters, so it was necessary to restart the simulations to observe the low altitude resonance behavior. Prior to low altitude resonance, the simulations were restarted without transients using the velocity, the flight path angle, and the trim angle of attack from the $G = 1$ trajectory. Since the initial transients were eliminated, the buildup in total angle-of-attack magnitude shown in Figs. 7a and 7b is due only to trim magnification near resonance. Note that transients are intro-

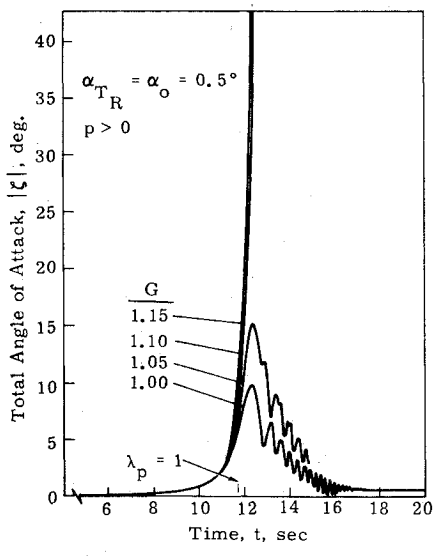

a) High altitude resonance encounter

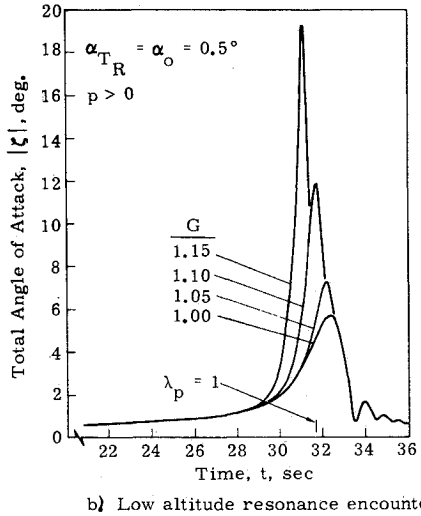

b) Low altitude resonance encounter

Fig. 7 Simulated (6-DOF) trim angle response to aerodynamic asymmetry and static moment slope asymmetry.

duced as the trim angle decreases rapidly from its maximum value.

The 6-DOF results presented in Fig. 7 confirm the analytical predictions concerning the effect of unsymmetrical static moment slope characteristics on trim angle magnitude. These results show that increasing the asymmetry of the static moment slope characteristics (increasing G in Fig. 7) increases the trim magnification near resonance. Theoretical results for these trajectory conditions predict an unbounded trim angle at the high altitude resonance encounter (Fig. 7a) when $G > 1.015$; while at the low altitude encounter (Fig. 7b), the trim angle is predicted to become unbounded when $G > 1.114$. Relative to the quasi-steady estimates, the effect of transient resonance is to increase the magnitude of the static moment slope asymmetry required for very unstable trim angle behavior to occur near resonance. This is demonstrated by the results given in Fig. 7.

In order to obtain an explosive divergence in trim angle with the 6-DOF results at the low altitude resonance encounter (Fig. 7b), it is necessary to increase the magnitude of G above the 1.15 value which is the upper limit for these simulations. The 6-DOF results presented in Fig. 7a for the high altitude encounter show that the explosive divergence in trim angle predicted by the theory begins between $G = 1.05$ and 1.10. Note that for $G = 1.10$ and 1.15 the trim angle is diverging rapidly. For these very unstable conditions, the large trim angles cause large drag decelerations ($300g$) which result in rapid decreases in both the pitch and yaw critical frequencies (p_{crp} and p_{cry}) through the effect of decreasing dynamic pressure. Because of the rapid increase in λ_p that resulted, the characteristic two peak trim magnification and jump discontinuities in windward meridian position indicated in Fig. 5 were not present in these simulations.

In order to simulate a two peak trim magnification and step changes in windward meridian position, G was increased to 1.50 and the reference trim angle, α_{T_R}, was decreased to 0.05°. Since the transient resonance condition tends to smear the responses to both resonances together, it was necessary to increase G. This created a very unstable condition near resonance; therefore, it was necessary to decrease the reference trim angle. The roll rate was maintained at a constant 3 Hz for these simulations. Under these conditions, even though the trim magnification was large, the vehicle was able to pass through pitch resonance without causing severe trajectory perturbations. As predicted by the theory, a step change in windward meridian position occurred. Near yaw resonance, the trim angle diverged explosively, once again causing a large decrease in dynamic pressure.

The results presented thus far make it obvious that the angular motion behavior of a vehicle with unsymmetrical static moment slope characteristics cannot be modeled accurately by using the average values of the stability derivative coefficients and assuming the vehicle is symmetrical. Because the trim magnitude and windward meridian behavior of these vehicles can differ greatly from that of a vehicle with symmetrical static moment slope characteristics, such an assumption will not allow a realistic evaluation of the vehicles' motion near resonance and may lead to erroneous predictions of trim induced roll rate behavior.

Conclusions

A quasi-steady analytical theory has been developed which describes the effects of unsymmetrical stability derivative characteristics on the trim angle behavior of slender rolling re-entry vehicles. Results presented in this article indicate that in addition to the usual dependence on aerodynamic damping, the magnitude and position of the trim angle of attack near resonance is heavily dependent on the asymmetry in the static moment slope characteristics. Unlike the effects of unsymmetrical aerodynamic damping, small differences in the static moment slope coefficients can result in very unstable trim angle behavior near resonance for re-entry vehicles that have small mass, aerodynamic and inertia trim producing asymmetries. Specific conclusions that can be drawn from the results presented here are as follows:

1) Increasing the asymmetry of the static moment slope characteristics increases the trim magnification near the resonances. When differences in the static moment slope coefficients exceed some altitude and aerodynamic damping dependent limit, unbounded trim magnification occurs near each undamped resonance accompanied by jump discontinuities in windward meridian position.

2) With unsymmetrical static moment slope characteristics the possibility of large trajectory dispersions and catastrophic vehicle failure may exist even with relatively small trim-producing asymmetries because of the large trim magnifications near resonance.

3) For vehicles with roll torques that result from a combination of c.g. offset and trim angle, large variations in roll rate behavior can be introduced by small changes in the asymmetry of the static moment slope coefficients.

4) The trim angle behavior near resonance for a vehicle with unsymmetrical static moment slope characteristics cannot be modeled accurately by using the average values of the static

moment slope coefficients and assuming that the vehicle has symmetrical stability derivative characteristics.

References

[1] Nicolaides, J. D., "On the Free-Flight Motion of Missiles Having Slight Configurational Asymmetries," Rept. 858, June 1953, U.S. Army Ballistic Research Lab., Aberdeen Proving Grounds, Md.

[2] Glover, L. S., "Effects on Roll Rate of Mass and Aerodynamic Asymmetries for Ballistic Re-Entry Bodies," *Journal of Spacecraft and Rockets*, Vol. 2, No. 2, March–April 1965, pp. 220–225.

[3] Pettus, J. J., "Persistent Re-Entry Vehicle Roll Resonance," AIAA Paper 66–49, New York, 1966.

[4] Platus, D. M., "A Simple Analysis of Re-Entry Vehicle Roll Resonance," TR-1001 (2240-30)-10, Jan. 1967, Aerospace Corporation, El Segundo, Calif.

[5] Barbera, F. J., "An Analytical Technique for Studying the Anomalous Roll Behavior of Re-Entry Vehicles," *Journal of Spacecraft and Rockets*, Vol. 6, No. 11, Nov. 1969, pp. 1279–1284.

[6] Price, D. A. and Ericsson, L. E., "A New Treatment of Roll-Pitch Coupling for Ballistic Re-Entry Vehicles," *AIAA Journal*, Vol. 8, No. 9, Sept. 1970, pp. 1608–1615.

[7] Hodapp, A. E., Jr. and Clark, E. L., Jr., "Effects of Products of Inertia on Re-Entry Vehicle Roll Behavior," *Journal of Spacecraft and Rockets*, Vol. 8, No. 2, Feb. 1971, pp. 155–161.

[8] Walchner, O., "Asymmetric Nose Bluntness Effects on the Aerodynamics of a Slender Cone at Mach 14," Paper 20, presented at the AIAA Second Atmospheric Flight Mechanics Conference, Palo Alto, Calif., 1972.

[9] Rhoads, D. W. and Schuler, J. M., "A Theoretical and Experimental Study of Airplane Dynamics in Large Disturbance Maneuvers," *IAS Journal of the Aeronautical Sciences*, Vol. 24, No. 7, July 1957, pp. 507–526.

[10] Bail, R. and Garner, H. C., "Calibration Models for Dynamic Stability Tests," Rept. 563, 1968, Advisory Group for Aerospace Research and Development, Neuilly-sur-Seine, France.